JOURNAL OF GEOPHYSICAL RESEARCH, VOL. 104, NO. B1, PAGES 1131–1150, JANUARY 10, 1999

High-resolution electromagnetic imaging of the San Andreas fault in Central California

Martyn Unsworth

Geophysics Program, University of Washington, Seattle

Gary Egbert

College of Oceanic and Atmospheric Sciences, Oregon State University, Corvallis

John Booker

Geophysics Program, University of Washington, Seattle

Abstract. Although there is increasing evidence that fluids may play a significant role in the earthquake rupture process, direct observation of fluids in active fault zones remains difficult. Since the presence of an electrically conducting fluid, such as saline pore water, strongly influences the overall conductivity of crustal rocks, electrical and electromagnetic methods offer great potential for overcoming this difficulty. Here we present and compare results from high-resolution magnetotelluric (MT) profiles across two segments of the San Andreas Fault (SAF) which exhibit very different patterns of seismicity: Parkfield, which has regular small earthquakes and creep events, and in the Carrizo Plain, where the fault is seismically quiescent and apparently locked. In both surveys, electric fields were sampled continuously, with 100 m long dipoles laid end-to-end across the fault. From 100 to 0.1 Hz the data from both profiles are consistent with a two-dimensional (2-D) fault-parallel resistivity model. When both transverse electric and magnetic (TE and TM) mode data are included in the interpretation, narrow (~300-600 m wide) zones of low resistivity extending to depths of 2-4 km in the core of the fault are required at both locations. However, at Parkfield the conductance (conductivity thickness product) of the anomalous region is an order of magnitude larger than at Carrizo Plain, suggesting much higher concentrations of fluids for the more seismically active Parkfield segment. We also image structural differences between the two segments. At Carrizo Plain, resistive, presumably crystalline, rocks are present on both sides of the fault at depths below 3-4 km. In particular, we clearly image resistive basement extending ~10 km or more east of the SAF, beneath the Elkhorn Hills and Temblor Range. At Parkfield the situation is quite different with a resistive block of Salinian granite west of the fault and an electrically conductive, presumably fluid rich Franciscan complex to the east. It is possible that these structural differences control the difference in mechanical behavior of the fault, either directly by affecting fault strength or indirectly by controlling fluid supply.

1. Introduction

Several lines of evidence suggest that high-pressure fluids in fault zones may play a critical role in controlling the rupture dynamics of earthquakes. First suggested by *Hubbert and Rubey* [1959], this concept gained support from the observation by *Zoback et al.* [1987] that in situ stress indicators, and the lack of significant heat flow anomalies [*Brune et al.*, 1969; *Lachenbruch*, 1980], imply that the San Andreas Fault (SAF) is inherently weak. Subsequently, *Willcock et al.* [1990] established that oceanic transform faults are also weak. While it is possible that the intrinsic weakness of strike-slip faults results from the presence of materials in the fault zone with a very low coefficient of friction, it is difficult to reconcile this explanation with laboratory-derived estimates of typical rock friction coefficients [*Byerlee*, 1978]. As a result, low intrinsic fault strengths have most often been explained in terms of high pressure fluids in the fault zone [e.g., *Sleep and Blanpied*, 1992; *Byerlee*, 1990, 1993; *Rice*, 1992]. This interpreta-

Paper number 98JB01755.
0148-0227/99/98JB-1755$09.00

tion is supported further by geological mapping of exhumed faults, which provides direct evidence that fluids were once present in zones of active strike-slip deformation [e.g., *Sibson et al.*, 1988; *Chester et al.*, 1993].

Zoback et al. [1987] demonstrated that simple models of overpressured fluids in the crust are inconsistent with in situ stress observations. To avoid unobserved hydrofracturing, fluid pressures would have to be limited by the minimum principal stress. To overcome this, and related difficulties, more sophisticated and detailed theoretical models for the dynamical behavior for fluids in mature active fault zones have been proposed [*Sleep and Blanpied*, 1992; *Byerlee*, 1990, 1993; *Rice*, 1992]. Although differing in many important details, these models all suggest a rather complicated picture in which the distribution, connectivity, and pressure of fluids may vary dramatically in space and time, in a manner which is closely linked to the earthquake cycle on individual fault segments.

To distinguish between theoretical models such as these, it is necessary to map the location of fault zone fluids in detail. While deep drilling such as that proposed by *Hickman et al.* [1994] will ultimately be needed to determine the physical state within the cores of active faults, remote sensing techniques capable of detecting in situ fluids to a depth of at least 10 km are clearly useful. *Eberhart-Phillips et al.* [1995] reviewed the resolution that might be obtained by seismic, electrical, and electromagnetic techniques. Since the presence of an electrically conducting fluid, such as saline pore water, strongly influences the overall electrical conductivity of crustal rocks, electrical and electromagnetic methods offer great potential for detecting fluids at depth within the fault zone. Electromagnetic exploration methods can be divided into those using natural sources such as magnetotellurics (MT) and those that require the generation of artificial electromagnetic signals. Electromagnetic signals propagate as loss free waves in the atmosphere but diffuse as highly attenuated waves in the ground which can generally be considered a good conductor. This attenuation is characterized by a skin depth $\delta = (2/\mu\omega\sigma)^{1/2}$, where ω is the frequency of the signal, μ is the magnetic permeability, and σ is the conductivity of the earth. To explore deep structure requires large skin depths and usually low-frequency signals. Such signals are difficult to generate artificially, but for most frequencies below 100 Hz, natural source signals are often strong. MT is thus generally used for crustal scale sounding.

In recent years, MT profiles have crossed the San Andreas Fault at a number of locations. *Park et al.* [1991] collected widely spaced long-period sites from the Pacific Ocean to Nevada, with one profile crossing the San Andreas Fault close to Parkfield. This study suggested that the Great Valley was bounded by electrically conductive suture zones but that the San Andreas Fault was not a significantly conductive feature in the lower crust and upper mantle. Based on U.S. Geological Survey MT data collected in the Parkfield area, *Eberhart-Phillips and Michael* [1993] inferred a significant resistivity contrast across the San Andreas Fault, with conductive material east of the fault. Unpublished USGS data (W. D. Stanley, personal communication, 1994) suggested that situation at Carrizo Plain was reversed, with an unexpected resistive body east of the San Andreas Fault beneath the Temblor Range. *Mackie et al.* [1997] imaged a similar pattern of resistivity variations along two additional profiles across the fault within the Carrizo Plain. These surveys used data collected at sites several to tens of kilometers apart. Although they have imaged large-scale contrasts in crustal resistivity across the fault and have sometimes provided indirect evidence for enhanced conductivity within the fault zone, sampling was not dense enough to provide a detailed view of the actual fault zone.

In this paper we describe the results of two high-resolution electromagnetic surveys across distinct segments of the San Andreas Fault where the earthquake cycle is very different: at Carrizo Plain and at Middle Mountain, Parkfield (Figure 1). In these surveys we sampled the electric fields on the surface with a continuous series of dipoles laid end to to end. This style of continuous MT profiling gives a high spatial data density and minimizes the possibility of spatial aliasing of

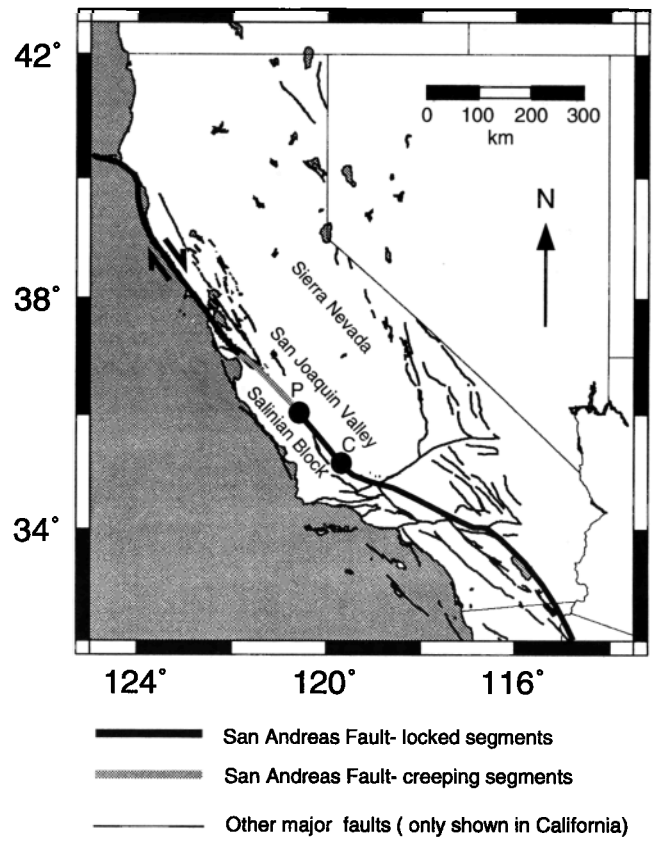

Figure 1. Map showing San Andreas Fault and the locations (solid dots) of continuous MT profiles at Carrizo Plain (C) and Parkfield (P).

near-surface static shifts into deeper structure [*Torres-Verdin and Bostick*,1992]. The method allows us to obtain high-resolution images of electrical conductivity variations within and near the fault zone to depths of around 4-6 km. Experimental details are provided in section 2. We then present and interpret results from modeling and inversion of the MT data for each profile. As we shall show, there are significant differences in geoelectric structure between the locked Carrizo segment and the Parkfield segment which has regular small earthquakes and creep events. In section 5 we consider possible implications of the different conductivity structures for fault dynamics.

2. Data Acquisition and Time Series Analysis

Data were collected using two Electromagnetic Instruments Incorporated MT-1 systems. The first system recorded 10 channels of data, including the horizontal magnetic fields at the center of each array, and electric fields for five along-profile and three across-profile dipoles. The layout is illustrated and contrasted with the conventional MT layout in Figure 2. Along the profile, dipoles were laid end-to-end, so that a continuous profile of electric fields was obtained across the fault. At Carrizo Plain, 100 m dipoles were used close to the fault, with 300 m dipoles at the ends of the profile. At Parkfield, 100 m dipoles were used throughout the survey. The second instrument was used to simultaneously collect standard five-channel MT data at a permanent site to permit remote reference processing of the time series data [*Gamble et al.*, 1979]. The remote site for the Carrizo Plain profile was located ~5 km from the southwest end of the profile; at Parkfield the remote reference was ~15 km from the profile. Data were recorded at each location overnight so that 500 to 1500 m of profile were covered per day.

Time series data were analyzed using the robust processing code of *Egbert* [1997] (a multiple-station extension of the method of *Egbert and Booker* [1986]) to compute estimates of the MT impedance tensor for frequencies between 100 and 0.005 Hz. In general, data quality was very good, except in the frequency range 1-0.1 Hz. In this "dead band" a combination of low MT signal strength, noise in the magnetic channels due to ground motion, and coherent cultural noise makes collection of high-quality MT data difficult. For these frequencies the remote reference estimates proved essential to remove downward bias in impedance magnitudes due to excessive noise in magnetic field components. Multiple station processing using the approach of *Egbert* [1997] detected low levels of coherent noise in narrow frequency bands near 4, 2, and 8 s. Curiously, noise in these same bands was found for both the Carrizo Plain and Parkfield profiles. The source of this noise remains unclear. Reprocessing with the robust multiple-station approach reduced the effects of this coherent noise somewhat, but estimates at these frequencies still show more scatter for some arrays and generally have larger error bars. However, these effects are confined to relatively narrow bands. Comparison to results for neighboring fre-

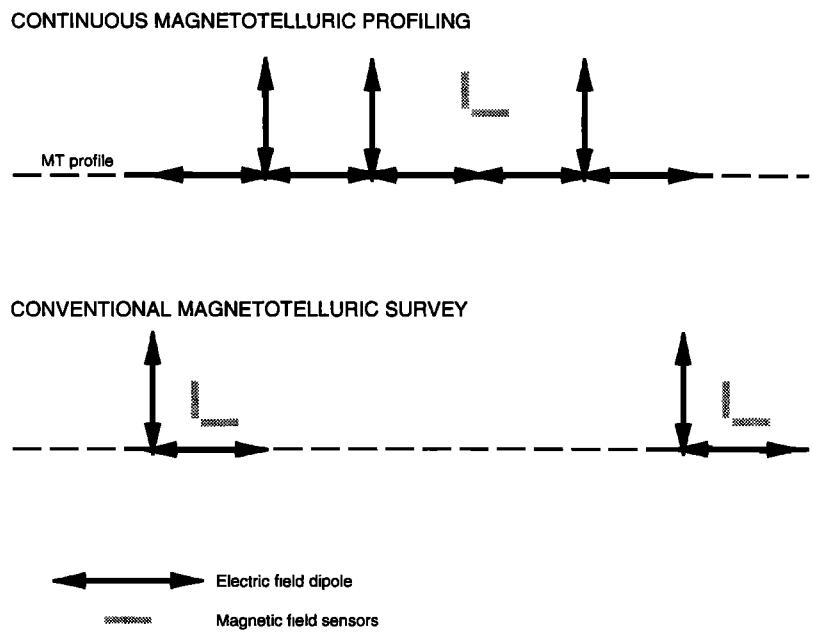

Figure 2. (top) Layout of electric dipoles and magnetic sensors used for electromagnetic array profiling, (bottom) compared to conventional MT survey configuration. The eight dipoles displayed for the continuous MT profile are recorded simultaneously in a single array. Additional arrays were laid out end-to-end to allow continuous along-profile sampling of the electric fields. Close to the fault, electric field dipoles were 100 m in length; farther away, they were 300 m.

quencies, where no coherent noise was detected showed that the impedances were not significantly biased by this noise.

At Parkfield the remote site failed after the first two arrays had been completed. It was thus not possible to compute standard remote reference estimates for most of this profile. To reduce bias in the dead band impedances, we again used the multivariate approach of *Egbert* [1997]. This scheme automatically computes estimates of signal-to-noise ratio for each channel, allowing unbiased estimates of impedances to be computed from an eigenvector decomposition of the spectral cross product matrix [*Park and Chave*, 1984]. Although developed for multiple-station processing, it can be shown that this scheme should also work well with the 10-channel MT profiling data considered here. In effect, the replicated electric field components can be used for the remote. As a check, results obtained by this approach were compared to robust remote reference results for the first two arrays, where a remote reference was available. In general, no consistent biases are observed in this comparison, so we believe the results for the full Parkfield profile are unbiased, even in the dead band.

3. Carrizo Plain

The San Andreas Fault at Carrizo Plain (Figure 1) is crossed by numerous offset creeks which clearly define the right-lateral offset of the fault. This segment has been locked since the 1857 Fort Tejon earthquake, and seismicity has been minimal since the advent of modern instrumentation [*Hill et al.*, 1990]. The Cretaceous Salinian block lies to the west of the fault with granitic and metamorphic crystalline basement overlain by 1-4 km of predominantly nonmarine Tertiary sedimentary rocks [*Dibblee*, 1973a,b; *Page*, 1981]. Several authors have suggested that the crustal block west of the San Andreas is not part of the Salinian block [*Ross*, 1984; *Irwin*, 1990]. The so-called Barret Ridge Slice appears to have an origin similar to the crystalline rocks of the San Gabriel Mountains to the south.

East of the San Andreas Fault, Cretaceous to Tertiary marine sedimentary units are exposed in the Temblor Range, and thrusting and folding indicates fault-normal compression [*Dibblee*, 1973a,b; *Page*, 1981; *Ryder and Thomson*,1986]. Extensive mapping and well log data in the oil fields of the eastern Temblor Range have shown that up to 7.5 km of sedimentary units underlies the Elk Hills some 15 km east of the San Andreas Fault [*Fishburn*, 1990]. Farther east, seismic refraction data have shown up to 12 km of sedimentary rocks in the Great Valley [*Colburn and Mooney*, 1986]. However, the character and depth of basement between the oil fields and the San Andreas Fault (i.e., beneath the Temblor Range) remain uncertain. It is assumed that the wedge of Franciscan formation that abuts the fault to the north is also present here (e.g., *Ryder and Thomson* [1986] show Franciscan at a depth of 3 km beneath the Temblor Range), but there is little direct evidence for its presence. Previous MT surveys in the Carrizo Plain detected resistive basement at depths less than 3 km beneath the Temblor Range [*Mackie et al.*, 1997; W.D. Stanley, personal communication, 1994.]

In the absence of microseismicity, the location of the San Andreas Fault at depth is uncertain. Recent geomorphic studies by *Arrowsmith* [1995] suggested that a vertical fault to a depth of several kilometers is required to explain uplift of the Elkhorn Escarpment. Seismic reflection and well log data to the southwest of the San Andreas were interpreted by *Davis et al.* [1988] to show that the Morales thrust shallows with depth and the resulting horizontal detachment may have offset the San Andreas 5-14 km to the east at depths of 5-7 km.

3.1. Dimensionality and Distortion Analysis

After the time series analysis described above, the dimensionality of the MT data was investigated using the tensor decomposition technique of *Chave and Smith* [1994]. Frequency-independent strikes were computed for four frequency bands for each array (i.e., the five MT sites collected each day). The misfit between the impedance predicted by the distortion model and the measured impedance was computed for strike angles from 0° to 90° in terms of a root mean square (rms) misfit. The strike angles that minimized the rms misfit for each array are shown in Figure 3. In the high-frequency band (100-10 Hz) the best fitting strike is 8° east of the surface trace, but a significant scatter occurs east of the surface trace. In the middle-frequency bands (10-1 Hz and 1-0.1 Hz) there is little variation between arrays, and strikes are within 5° of the fault trace. The lowest frequency band (0.1-0.01 Hz) shows a consistent strike 25° west of the fault strike. Figure 4 shows how well the decomposition model fits the impedance data for site 30 at Carrizo Plain. In the three high-frequency bands (100 to 0.1 Hz) the impedances are fit to within a rms normalized misfit in the range 1-5. At lower frequencies, in the 0.1-0.01 Hz band, the two-dimensional (2-D) distorted model does not fit well, with rms misfits from 10-50. This poor fit indicates a 3-D regional structure and is consistent with the change of strike at these frequencies. Fits to the distorted two-dimensional model for the other sites were similar. Figure 5 shows the impedance skew for all sites. Above 0.1 Hz most skews are less than 0.1, again suggesting a 2-D geoelectric structure. Below this frequency, skew becomes large indicating a 3-D geoelectric structure is being sensed.

The small skew values and uniform strike at frequencies between 100 and 0.1 Hz suggests that the MT data are consistent with a two-dimensional (2-D) interpretation, in a fault normal and parallel coordinate frame. Data from 0.1 to 0.01 Hz should be included only with caution, particularly if interpreted in the same coordinate frame. The change of strike estimated for this

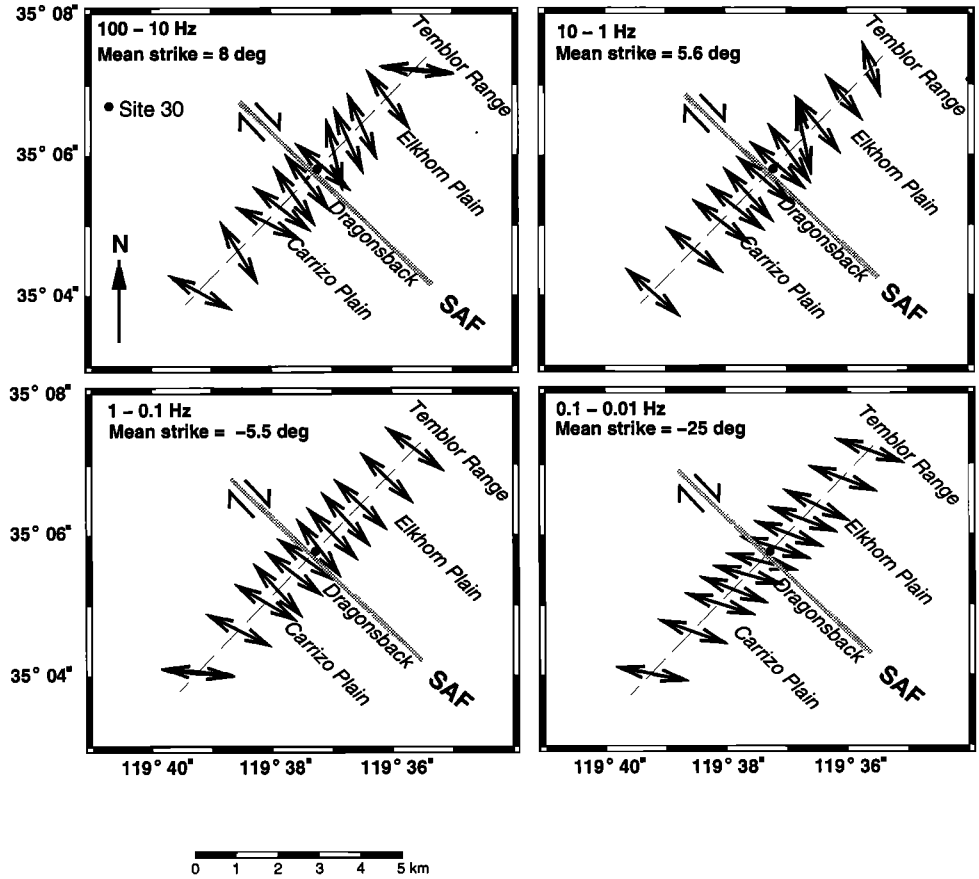

Figure 3. Map of continuous MT profile at Carrizo Plain with arrows for each array showing best fitting 2-D strike direction in four frequency ranges. Except for the lowest-frequency band the geoelectric strike is consistently within 5°of the surface fault trace.

last band and the increased misfit to the 2-D distorted model suggest that there may be some contamination by three-dimensional (3-D) effects at long periods, where the MT data sample a larger volume. In particular, the deep strike (25°W of the surface trace) may reflect the

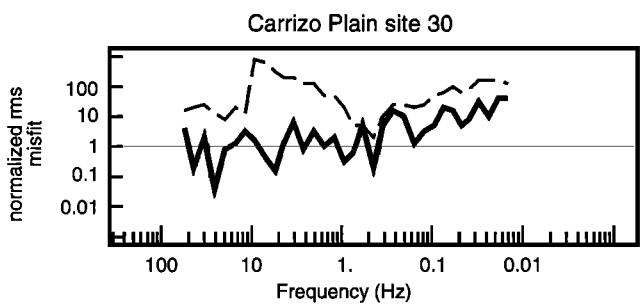

Figure 4. Fit of data to decomposition model for site 30 at Carrizo Plain. The solid curve indicates the minimum misfit that occurs as strike is rotated from 0° to 90°. An ideal minimum misfit would be 1. The dashed curve indicates the maximum misfit. When minimum and maximum misfit are similar in value there is limited control on strike, when different the strike is well constrained.

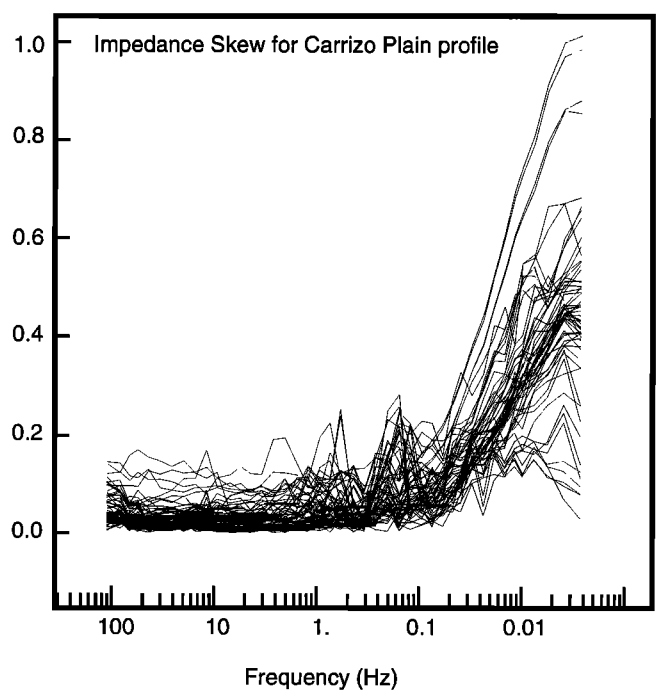

Figure 5. Impedance skew for the all sites on the Carrizo Plain profile.

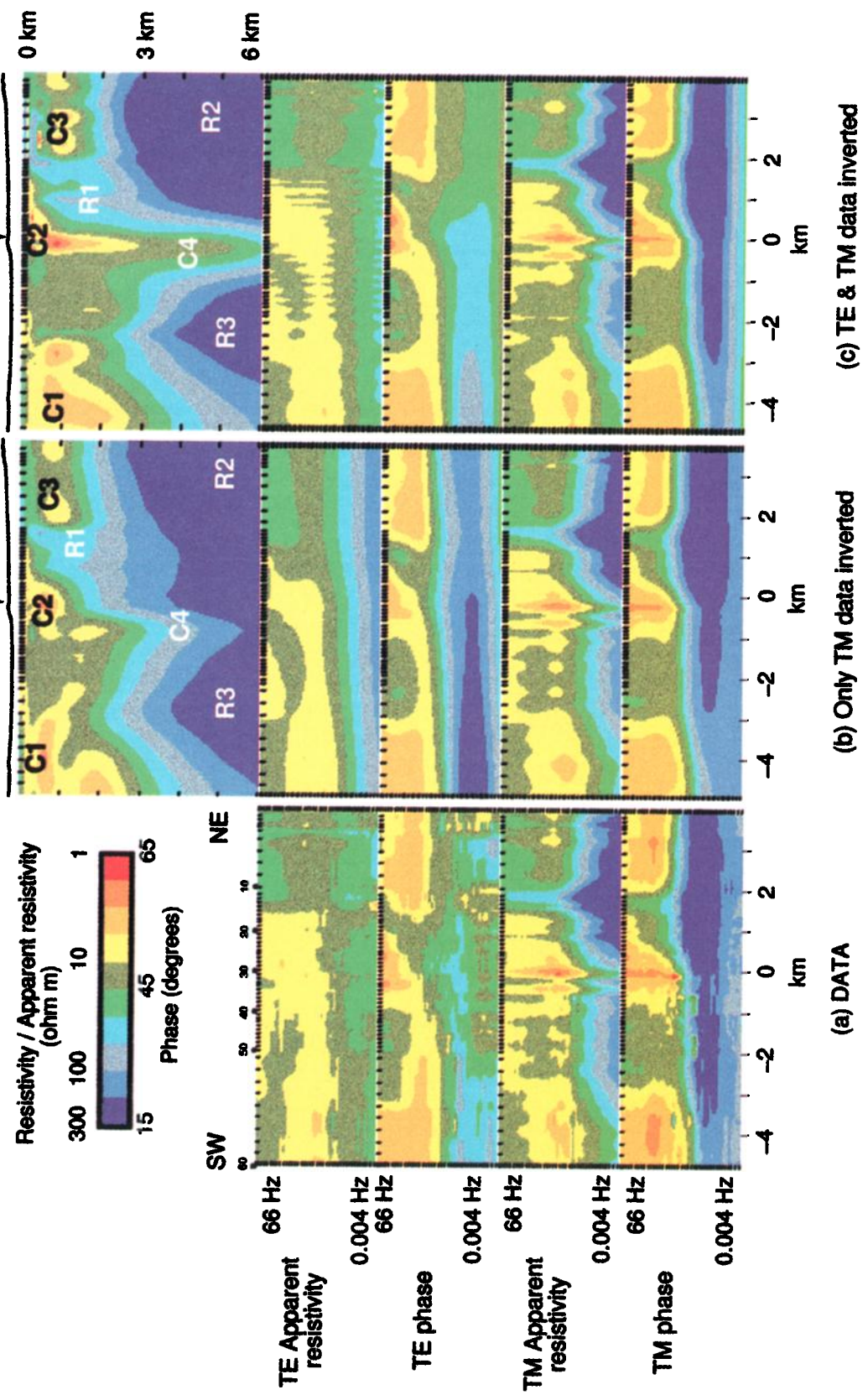

Plate 1. (a) Data pseudo-sections for Carrizo Plain MT profile. (b) Resistivity model and model response obtained by inverting TM data. (c) Resistivity model and response that fits both TE and TM data. The topographic profile is shown at the top of the figure. Models and topography are plotted with no vertical exaggeration. Major conductive (C1-C4) and resistive (R1-R3) features discussed in the text are indicated in Plates 1b and 1c.

change in direction of the San Andreas to the southeast of the Big Bend or the surface geologic strike of the Cuyama valley and related faults to the south [*Page*, 1981]. Alternatively, these indications of 3-D complications could reflect the change in direction of the coastline in southern California.

The resulting apparent resistivity and phase data in a fault parallel (i.e. unrotated) coordinate system are shown in Plate 1a. The horizontal ticks denote the centers of the electric field dipoles, and frequency is shown on the vertical scale. Because of the skin depth effect noted above, this pseudo-section gives a sense of how the structure varies with depth. TE mode apparent resistivity and phase correspond to electric currents flowing along the fault, while the TM mode data correspond to electric currents flowing normal to the fault.

3.2. Modeling and Inversion

The apparent resistivity and phase data were converted into a spatially smooth electrical resistivity model using a combination of inversion and forward modeling. The rapid relaxation inversion (RRI) of *Smith and Booker* [1991] was applied in the following steps:

1. Horizontally average TM apparent resistivity (ρ_{TM}) and phase (Φ_{TM}) data, and invert for a 1-D layered Earth model. At each frequency an average ρ_{TM} and Φ_{TM} was computed for all sites on the line. This procedure allowed the inversion in step 2 to converge more rapidly than if started from a half-space.

2. Using this model as a starting point, begin a 2-D inversion to fit the TM data (ρ_{TM} and Φ_{TM}). The resulting model and computed response are shown in Plate 1b. Note that the actual model used extended 300 km to the east and west and included the Pacific Ocean as a fixed feature, to allow for the significant effects of the highly conductive ocean on MT measurements made onshore [e.g., *Ranganayaki and Madden*, 1980: *Mackie et al.*, 1988]. The TM mode data are fit well, to a normalized rms misfit of 2.1. This corresponds to misfits of individual data of $\approx$ 10 percent for apparent resistivities, and 5° for phases. Note that ideally misfits would be equal to the standard errors in the data i.e., the rms misfit would be 1. However, the TE response of this model does not fit the data below a frequency of 1 Hz.

3. A two-dimensional inversion was started from the model obtained in step 2 and required the TE apparent resistivity (ρ_{TE}) and phase (Φ_{TE}) to be satisfied in addition to the TM mode data. The RRI algorithm was unable to significantly lower the misfit for the combined data set because it was trapped in a local minimum of the data misfit function. Using trial-and-error forward modeling to improve the fit to the TE responses without significantly altering the TM response, we found that both TE and TM mode data could be fit reasonably well by the addition of the large conductor east of the profile that was imaged in previous regional MT surveys by *Mackie et al.* [1997] and W. D. Stanley (personal communication, 1994). Given the way in which the RRI algorithm searches model space and the lack of data on the east end of profile, it is not surprising that this better fitting model was not found by the inversion scheme alone.

4. A final inversion was started from this hybrid model, resulting in a combined rms misfit of 2.6 for both modes. The model and its response are shown in Plate 1c . The vertical stripes in ρ_{TE} are due to the application of frequency-independent static shift coefficients that were computed by the inversion and displayed in Figure 6a. Allowing the inversion to estimate

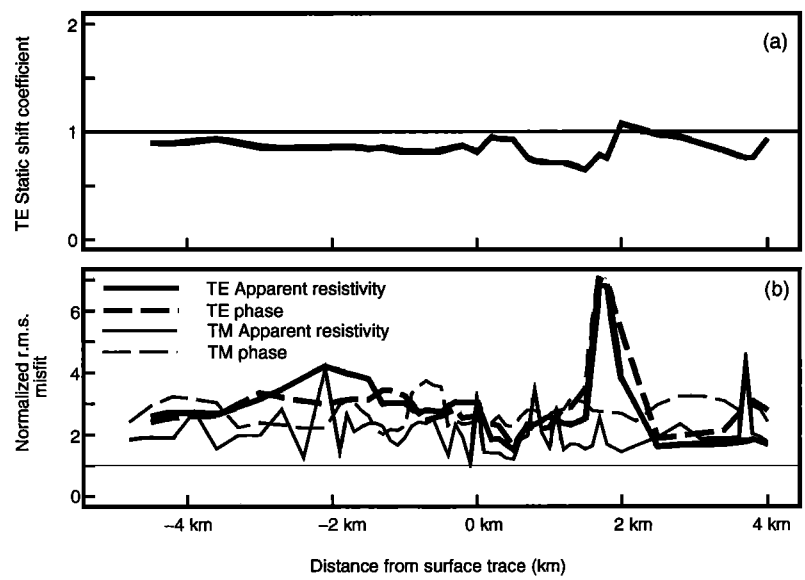

Figure 6. (a) Estimated static shift coefficients for the Carrizo Plain data. (b) Misfit between data and predicted response of model in Plate 1c as a function of distance from the surface trace.

static shifts effectively downweights the resistivity data, making the interpretation less susceptible to distortion by galvanic effects and is equivalent to the technique of manually "correcting" for static shift. Note that both modes are generally fit well down to a frequency of 0.1 Hz. Below this frequency the predicted phases are higher than the observed. This may reflect the fact that a 2-D fault-oriented model is invalid at these frequencies, as implied by the tensor decomposition and skew values. The normalized rms misfits for each site are shown in Figure 6b. Misfit levels are relatively uniform across the profile, except for two adjacent sites 2 km east of the fault trace. This poor fit to the TE data is almost all due to the very poor fit for the lowest frequencies (0.1-01 Hz) and probably reflects a combination of local distortion and the change of strike direction at these frequencies.

A similar model was obtained by the inversion sequence: (1) Fit TE data starting from a 10 Ω m halfspace; and (2) from this model, fit both TE and TM mode data. This gave a good fit to the TE data by placing the conductive structure at depth east of the profile but did not fit the small-scale structure required by the TM data at high frequencies. While some details in the geometry vary, both the TM data and TE+TM data models have the following conductive (C) and resistive (R) features in common:

C1, 5-10 Ω m conductive layer west of the surface trace of San Andreas Fault; C2, 3-7 Ω m conductive zone beneath the surface trace in the upper km; C3, 7-20 Ω m conductive layer at the east end of the profile; C4, Zone of slightly enhanced conductivity beneath the fault trace; R1, 50-100 Ω m resistive, westward dipping layer; R2, 300-1000 Ω m resistive basement below 2 km east of fault; R3, resistive basement below depth of 3-4 km west of San Andreas Fault.

The differences between the TM and TE+TM models can be understood by considering the physics of 2-D MT. Thin vertical conductors are essentially invisible to TM mode electric currents. Positive and negative electric charges develop on opposite sides of the conductor at depth, but the effect of these charges largely cancels out at a location on the surface. However, TE mode electric currents flowing along the conductor are readily detectable on the surface, even if the body is very narrow. Thus the Carrizo Plain TM data are sensitive to the contrast in resistivity across the fault but do not require a significant fault zone conductor below 2 km. In contrast, the TE data are more sensitive to the presence of the narrow conductor (C4) in the fault zone, which extends in the combined TE+TM model to a depth of 6 km.

It is important to consider the possibility of 3-D effects. One possible source of 3-D effects is the shallow, but very conductive basin partly occupied by Soda Lake at Carrizo Plain. This could systematically distort the electric fields so that large static shift coefficients would be required to fit ρ_{TE}. However, estimated static shifts are small (Figure 6a), indicating that strong distortion of the whole profile is unlikely. Furthermore, this type of distortion has less effect on the phase, which we have emphasized in our inversion. The 3-D effects could also result from conductive structures (e.g., C4) with limited continuity along strike. In this case the TM response would be virtually unaltered, but ρ_{TE} could be artificially lowered by electric charges developing at the ends of the conductor [*Wannamaker et al.*, 1984]. A 2-D interpretation emphasizing ρ_{TE} could thus lead to an overestimate of conductance for the 3-D feature. Note, however, that this discussion presumes the existence of the conductive structure. It is the magnitude of the conductance, not the presence or absence of the feature which might be called into question by possible unresolved 3-D effects. Given the consistent geoelectric strike, the small skews, and the essential similarity of the TM and TE+TM models, we believe that a 2-D interpretation of this dataset is reasonable. However, it should be borne in mind that quantitative estimates of conductance for some features might be biased to some small extent by 3-D end effects.

3.3. Interpretation

Our interpretation of the Carrizo Plain resistivity model is summarized in Plate 2a. Note that faults can change the electrical resistivity of the ground in at least two distinct ways. They can produce a zone of low resistivity by trapping groundwater uphill of a fault and also by forming a zone of low resistivity in the gouge and breccia at the core of the fault.

3.3.1. Structure west of San Andreas Fault. The shallow conductivity structure is well-correlated with geologic mapping and well log data from the area. West of the fault, *Vedder* [1970] mapped the Wells Ranch syncline, consisting of Caliente formation sedimentary units [Plate 2a]. This corresponds to conductive unit C1, and the westward dipping resistivity contours between 3 and 5 km west of the SAF correlate well to the dip of the eastern limb of the syncline. At a depth of ~4 km the resistivity increases significantly (R3), presumably corresponding to crystalline basement of the Salinian block. The location of this boundary inferred from seismic reflection by *Davis et al.* [1988] agrees well with the resistivity model. *Davis et al.* [1988] suggest this contact is a back thrust fault (F4) associated with the deeper Morales thrust, whose inferred location is shown in Plate 2a.

3.3.2. Shallow structure east of San Andreas Fault. Immediately to the east of the surface trace is a wedge of low resistivity (C2) with its western boundary directly beneath the surface trace. Note that the surface trace lies just east of the change in elevation associated with the Dragonsback pressure ridge. Mapping and well logs compiled by *Vedder* [1970] indicate that C2 is the Bitterwater Creek shale, a clay rich sequence with low electrical resistivity. Trapping of groundwater uphill (east) of the fault may also contribute to the low

resistivity. *Arrowsmith* [1995] found a number of fault-controlled springs in this area, consistent with the idea that fault can act as a barrier to groundwater flowing from the northeast in the near surface. Farther to the east, R1 correlates with the Santa Margarita formation, described by *Vedder* [1970] and *Dibblee* [1973a,b] to be a sedimentary unit containing granite boulders up to 12 ft in diameter, in addition to gneiss and other clasts. This may account for the relatively high resistivity of this unit, and the boundaries (inferred to be thrust faults) correlate well with the spatial extent of the central shallow resistive zone. Near the eastern end of the profile, C3 is interpreted as a sandy-clay rich facies of the Monterey shale which also has a low resistivity. Note that there are two distinct zones of low resistivity, and that both of these lie east of, and topographically above, the thrust faults (F2 and F3) mapped by *Vedder* [1970] and *Ryder and Thompson* [1986]. Concentrations of groundwater trapped by these faults, may contribute to the low resistivities imaged along the MT profile.

3.3.3. Resistive basement east of San Andreas Fault. The most striking feature east of the fault is the shallow depth ($\sim$ 2 km) to resistive basement ($>$ 300 Ω m). Seismic reflection and MT data at Parkfield [*Unsworth et al.*, 1997a] showed that the top of the Salinian granite corresponded to the 100 Ω m contour. This suggests a crystalline basement at a depth of 2 km beneath the Elkhorn Hills and Temblor Range east of the San Andreas. However, this interpretation is at variance with currently accepted tectonic models of this area [*Page*, 1981] in which Great Valley sedimentary units and the Franciscan formation extend westward to the San Andreas Fault. These rock units would be expected to have a lower resistivity than the 200-3000 Ω m observed, although *Park et al.* [1991] reported resistivities greater than 500 Ω m in the Franciscan formation, possibly due to greenstones or metabasalts. Significantly, *Graff* [1962] reports that the Western Gulf Oil Vishnu No. 1 well (located some 6 km along strike from our profile on the northeast side of the San Andreas) bottomed at 2114 m in granite. This resistive unit has also been detected by previous MT surveys that crossed the San Andreas Fault at several locations within Carrizo Plain [*Mackie et al.*, 1997; W.D. Stanley, personal communication, 1994]. Thus the resistive feature is neither a local structure confined to a single profile, nor an artifact of the data acquisition and processing reported here.

How far east does the resistive structure extend? It certainly extends to the eastern end of the profile, and beyond this point our data provide minimal control but are still sensitive to some structure at depth. During the inversion process described above, it was found that to fit the essentially flat ρ_{TE} responses, lower resistivity material was required somewhere to the east of the profile and that the resistive basement block could be terminated $\sim$6 km east of the SAF and not shown in Plate 2a). This was confirmed by *Mackie et al.* [1997], who collected MT data at a site east of the Temblor Range. Thus the resistive unit is most likely only a horizontally limited sliver of crystalline rock. Clearly, it does not extend into the oil fields east of the Temblor Range, where wells have penetrated up to 7.5 km in sedimentary rocks of the Great Valley sequence [*Fishburn*, 1990].

While *Zoback et al.* [1987] showed that the San Andreas is inherently weak, *Castillo and Hickman* [1995] suggested that within 5 km of the San Andreas Fault the Carrizo segment is strong. Our data support this suggestion since it implies there is crystalline, presumably mechanically strong material on both sides of the fault below 2 km depth. The material to the west could be Salinian granite or, alternatively, crystalline basement of the Barret Ridge Slice. The material to the east is of undetermined origin. It could be a fault slice of Salinian granite or part of the Barret Ridge Slice, which is believed to originate in the crystalline basement that underlies the Mojave desert and San Gabriel Mountains [*Ross*, 1984; *Irwin*, 1990].

3.3.4. Fault zone conductor. In contrast to Parkfield (see *Unsworth et al.* [1997a] and also section 4) the SAF at this location is a relatively subtle feature of the resistivity model. Although the MT data are consistent with a modest reduction of resistivity in the fault zone, this feature is not particularly striking. In the upper kilometer the fault appears to act as a barrier to groundwater flow, as a zone of low resistivity is found east (on the uphill side) of the fault. Below this depth a zone of reduced resistivity extends to depths of at least 4 km. This feature could represent a weak fault zone conductor that has been smeared out by the inversion, as observed in synthetic MT model studies by *Eberhart-Phillips et al.* [1995]. However, the fault zone conductance (conductivity times fault zone width) at Carrizo Plain is of the order of only 20 S. This is an order of magnitude less than the 250 S fault zone conductance imaged at Parkfield which *Unsworth et al.* [1997a] interpreted as due to an anomalously high fluid concentration.

What is the maximum fault zone conductance consistent with the data? To explore this question, the best fitting model was modified by decreasing resistivity within the fault zone in a variety of ways. Figure 7 shows the observed TE mode data and the responses of selected models at site 30, which was typical of sites within 2 km of the surface trace. Adding a 100 m wide 2 Ω m fault zone conductor (i.e., 50 S conductance) lowers ρ_{TE} significantly below 0.5 Hz. Increasing the width to 300 m (150 S conductance) produces an even more unacceptable fit. Alternatively, increasing the resistivity of the fault between 1 and 3 km to 10 Ω m raises ρ_{TE} so that the data are not fit between 5 and 0.2 Hz. Note that the TM data for the same models shown in Figure 7 are much less sensitive to variations in fault zone conductivity. Thus the fault zone conductance is at least partially constrained by the TE data. However, as we

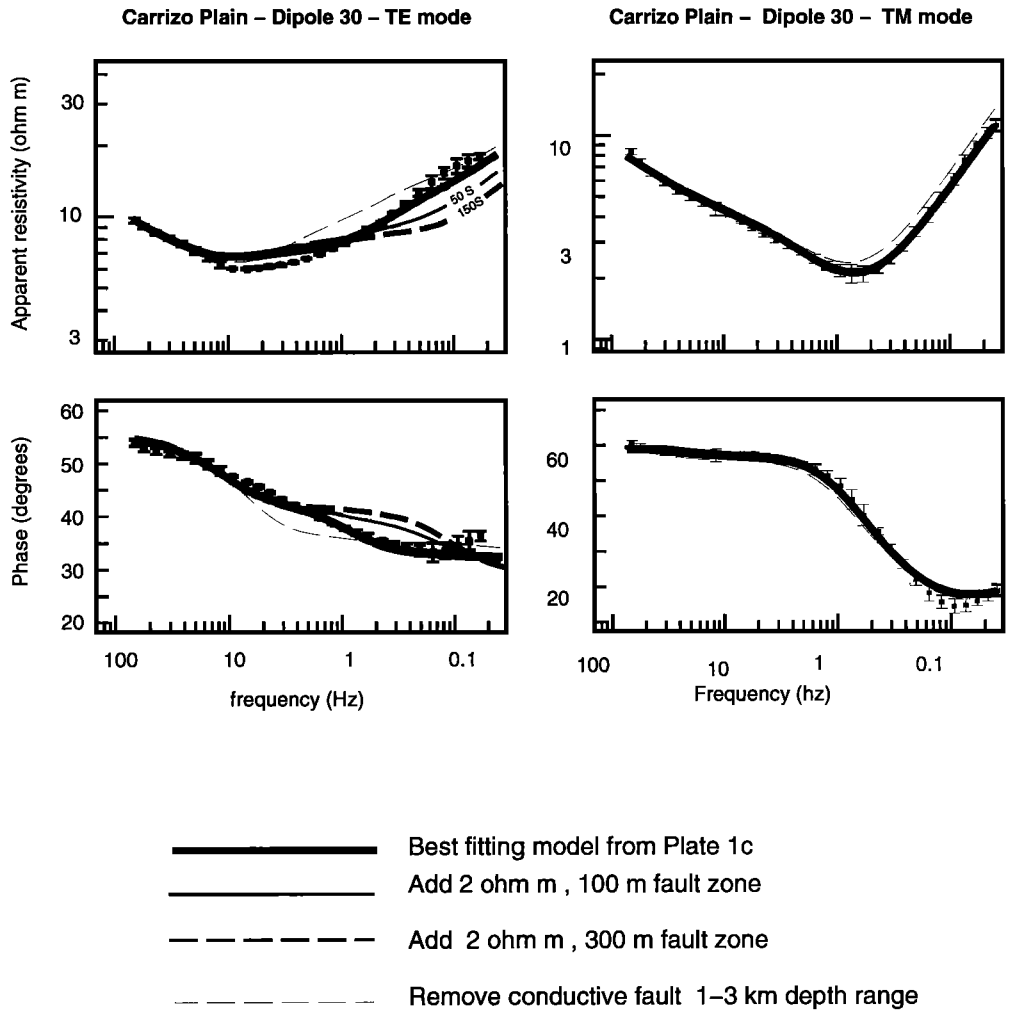

Figure 7. TE and TM mode responses and measured data at dipole 30 for a set of models including a more conductive fault zone. Note that the TM mode data are virtually insensitive to the fault zone conductance, while the TE data constrain this quantity.

have discussed in section 3.2, the possibility of 3-D end effects adds some uncertainty to quantitative estimates of fault zone conductance.

3.3.5. Faulting pattern. Shallow crustal deformation in the vicinity of the MT profile is dominated by a series of westward dipping thrust faults, denoted as F1-F4 in Plate 2a. In our interpretation the main vertical trace of the San Andreas Fault is offset laterally to the west by 200-300 m at a depth of around 500 m. Based on geomorphic mapping, *Arrowsmith* [1995] proposed a model for the uplift of the Dragonsback pressure ridge in the Elkhorn Hills, in which a thrust fault intersected and beheaded the originally vertical SAF at around 500 m depth. The inferred location of F1 correlates well with the near-surface zone of low resistivity in our model in Plate 2a. *Arrowsmith* [1995] estimated that an offset of around 200 m was needed to produce the necessary uplift. Again, this is in good agreement with the modeled location of the deeper fault zone conductor in Plate 2a. Note that fault F4 (inferred from the electromagnetically mapped location of the resistive basement contact) might be a continuation of F1 across the San Andreas Fault. The contact between C2 and R1 might be a thrust fault (F1) that offsets the San Andreas Fault to the west at around 1500 m depth.

Farther to the east, F2 and F3 are thrust faults mapped at the surface by *Vedder* [1970] and *Ryder and Thomson* [1986]. The locations of these faults within the upper 2 km of sedimentary rocks are strongly correlated with variations in the resistivity model [Plate 2a]. These faults may also penetrate the crystalline basement and possibly intersect the San Andreas at depth, but the MT data offer no supporting evidence for this possibility. Indeed, our model does not exhibit any significant vertical offsets in depth to the resistive basement beneath this part of the profile.

Can our data constrain the location of the San Andreas Fault at depth? The location of the Morales thrust inferred by *Davis et al.* [1988] is shown in Plate 2a. This resistivity model shows no evidence for conductive sedimentary units below this depth. Certainly, a horizontally limited feature at this depth is near the limits of what we might resolve with our 9 km long profile. The longer profile of long-period MT measure-

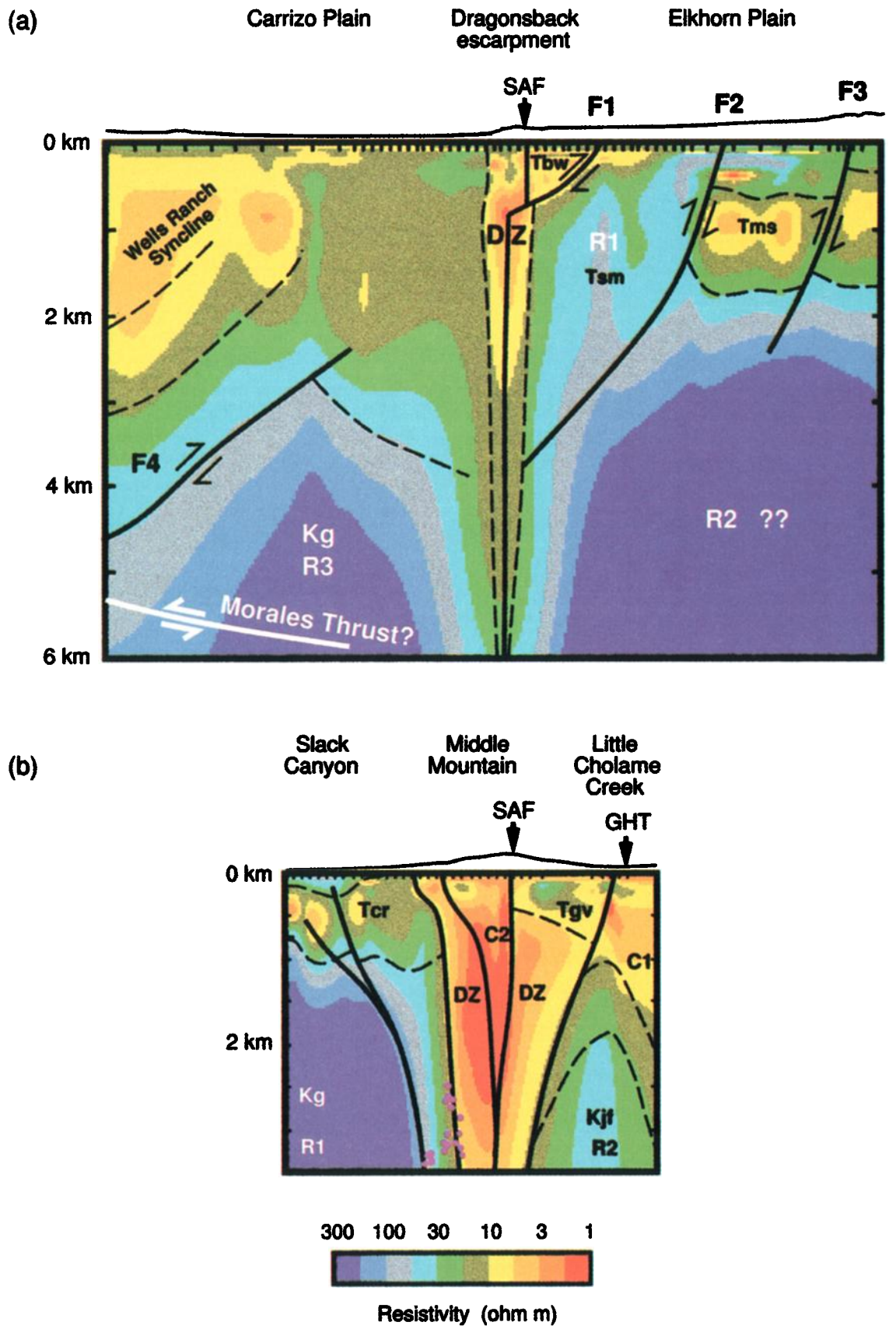

Plate 2. Interpretation of resistivity models. (a) Carrizo Plain with geologic units labeled as by Vedder [1970]: Kg, Salinian granite; Tbw, Bitterwater Creek Shale; Tms, Monterey shale; Tsm, Santa Margarita formation; DZ, damaged zone. See text for discussion of faults F1-F4. (b) Middle Mountain, Parkfield with geology east of the San Andreas Fault taken from *Sims* [1990]. Tcr, Tertiary Coast Range units; Tgv, Great Valley sequence; Kjf, Franciscan formation. GHT, Gold Hill thrust Fault. Dots denote earthquake hypocenters from the Berkeley seismic network. Models shown with no vertical exaggeration.

ments described by *Mackie et al.* [1997] also fails to image conductive structure below the inferred Morales thrust, suggesting that if the Morales thrust extends this far east as a subhorizontal detachment, it is most likely underlain by crystalline basement. However, it is possible that sediments thrust to 8 km depth might be only weakly conductive and that the conductive surface layer (C1 and C2) masks what would then be a relatively subtle feature in the MT data. There is also no clear evidence in either the resistivity model of Plate 2a or the model of *Mackie et al.* [1997] for an eastward offset in the San Andreas Fault at 8 km depth, as suggested by *Davis et al.* [1988]. However, even if a horizontal detachment is invisible to MT, the San Andreas Fault at depth might be imaged electrically. The midcrustal conductor detected east of Carrizo Plain by deep sounding data of *Biasi et al.* [1990] might correspond to the San Andreas Fault offset to the east at depth.

4. Middle Mountain, Parkfield

The seismic behavior of the Parkfield segment differs significantly from the Carrizo segment. Here there is extensive microseismicity, with the shallowest events occurring in repeating clusters at depths of ~3 km. Focal mechanisms, and the repeat sequence, suggest that seismicity is fluid driven [*Nadeau et al.* 1995 ; *Johnson and McEvilly*, 1995]. Characteristic $M \approx 6$ events have ruptured this segment on average every 22 years since 1857 [*Bakun and Lindh*, 1985]. In contrast to Carrizo Plain the location of the fault at depth is seismically well-defined and is close to vertical to a depth of 8 km. Previous studies of the Parkfield segment using both

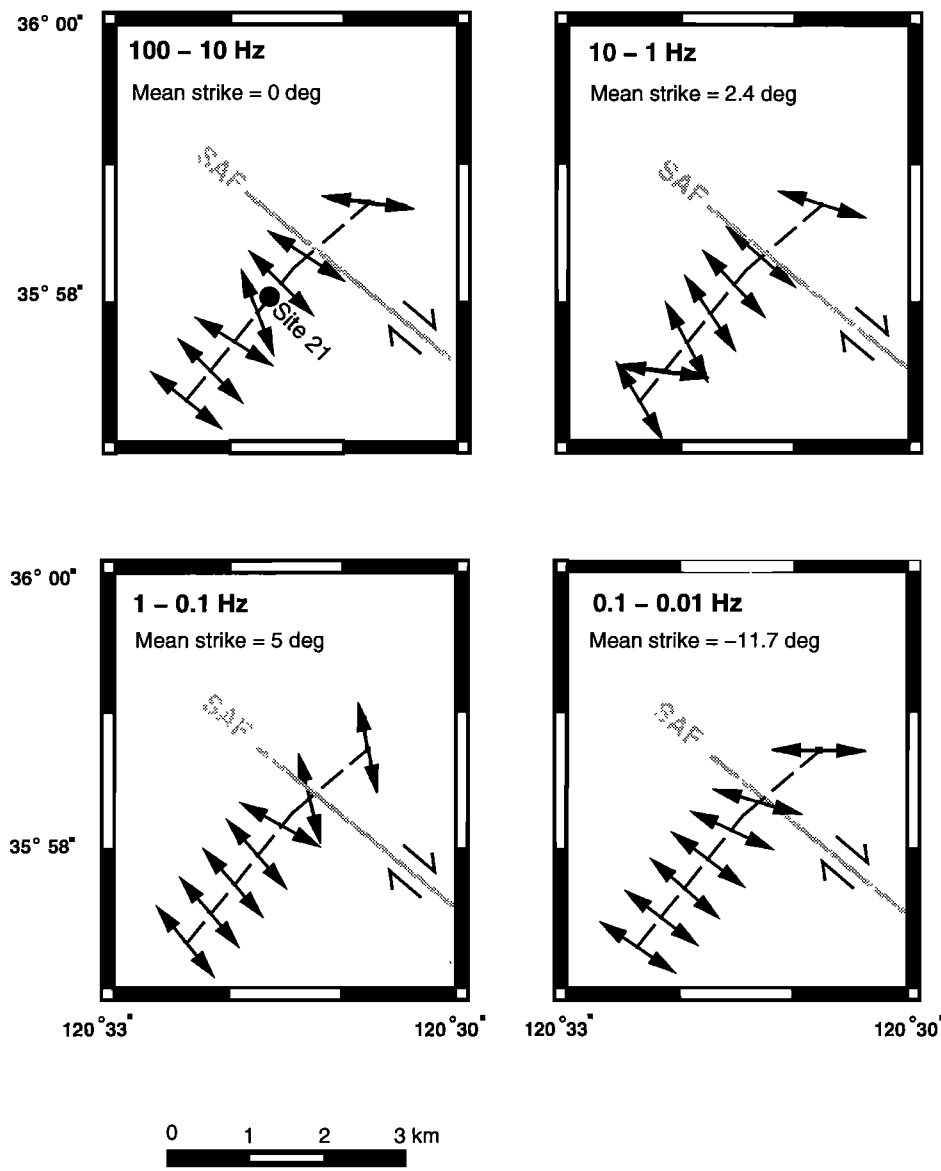

Figure 8. Map of continuous MT profile at Parkfield, with arrows showing best fitting 2-D strike direction for each array in four frequency ranges.

direct current (DC) electrical methods [*Park and Fitterman*, 1990] and MT [*Eberhart-Phillips and Michael*, 1993] suggest that electrical resistivities are low in and near this fault segment. The MT survey also revealed a broad (20+ km) wide zone of low resistivity in the upper 5 km of the crust northeast of the SAF. This zone was correlated with a pronounced seismic low-velocity zone [*Eberhart-Phillips and Michael*, 1993]. Our profile at Parkfield is only 4 km in length but is sampled densely enough to reveal significantly more detailed images of shallow fault zone resistivity structure than have been available previously. An initial interpretation of these data was given by *Unsworth et al.* [1997a], who showed that the fault zone was coincident with a relatively narrow (500 m wide) vertical zone of low resistivity, which was attributed to the presence of significant amounts of fluid. Here we provide a more detailed description of the inversion results and explore the range of possible models that are compatible with the data. We will show in particular that the TE data imply that the zone of low resistivity extends to a depth of 2-4 km.

4.1. Dimensionality and Distortion Analysis

Tensor decomposition was applied to the impedance data, following the procedure described in section 3.1, and results are presented in Figure 8. The decomposition model fits the data quite well in each of the four frequency bands. Although there is some scatter in the directions at shorter periods, the estimates of geoelectric strike for arrays west of the SAF are generally consistent and within $\pm 5°$ of the surface trace. East of the SAF the strike is less well-constrained as the TE and TM responses are relatively similar, in contrast to the west where they are very different. The fit of the decomposition model to the impedance data for a typical site (site 21) is shown in Figure 9. The minimum rms misfit can be seen to be acceptable at all frequencies. The impedance skews shown in Figure 10 are almost all below 0.2. Thus for the bulk of the profile the decomposition and skew analysis suggest that a 2-D interpretation will be reasonable over the whole frequency band. The TE and TM apparent resistivity and phase in this fault-oriented co-ordinate system are shown in Plate 3a in pseudo section format.

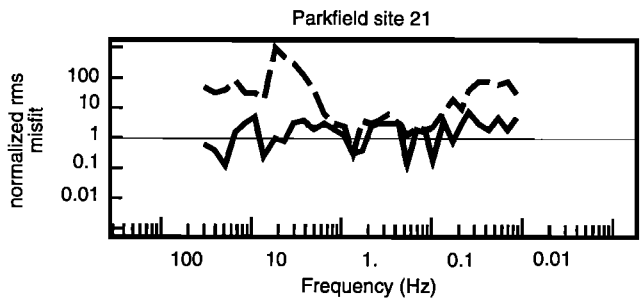

Figure 9. Fit of data to decomposition model for site 20 at Parkfield.

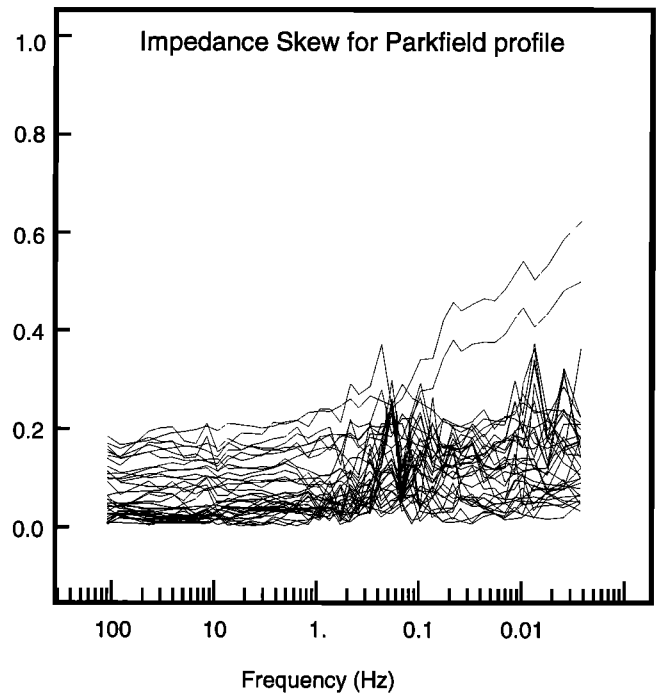

Figure 10. Impedance skew for all sites on the Parkfield profile

4.2. Modeling and Inversion

The data were inverted using a sequence similar to that described for the Carrizo Plain data. Inversion of the TM data produces the model shown in Plate 3b. This model fits the TM data well, but does not come close to fitting the TE data. To adequately fit both modes, the TM model was modified to improve the fit to the TE data. We found that a conductive layer of 1 Ω m, 1 km thick fixed in the model at a depth of 2 km, and located 4 km to the east of the SAF solved this problem. This closely matches the conductive zone east of the SAF mapped in previous MT surveys of this area [*Eberhart-Phillips and Michael*, 1993]. This model was used as a starting model for a joint TE+TM inversion using RRI. The model and response are shown in Plate 3c. Note that in the TE+TM model the fit to the TM data has been improved, particularly in Φ_{TM} east of the fault trace due to the addition of a resistive zone, R2. Again, the TM data image the contrast in resistivity across the fault at depth and also the top of the large fault zone conductor. However, the bulk of the fault zone conductor, C2, is invisible to TM data and is only imaged by the TE mode. The vertical stripes in the computed ρ_{TE} result from application of static shift coefficients (Figure 11a) to the responses. Static shifts are larger for Parkfield than for Carrizo Plain, probably in part due to topographic effects. Figure 11(b) shows that the rms misfit is uniform across the profile, with all sites fit comparably well.

As discussed for the Carrizo Plain data, interpretation of TE mode data must be undertaken with care

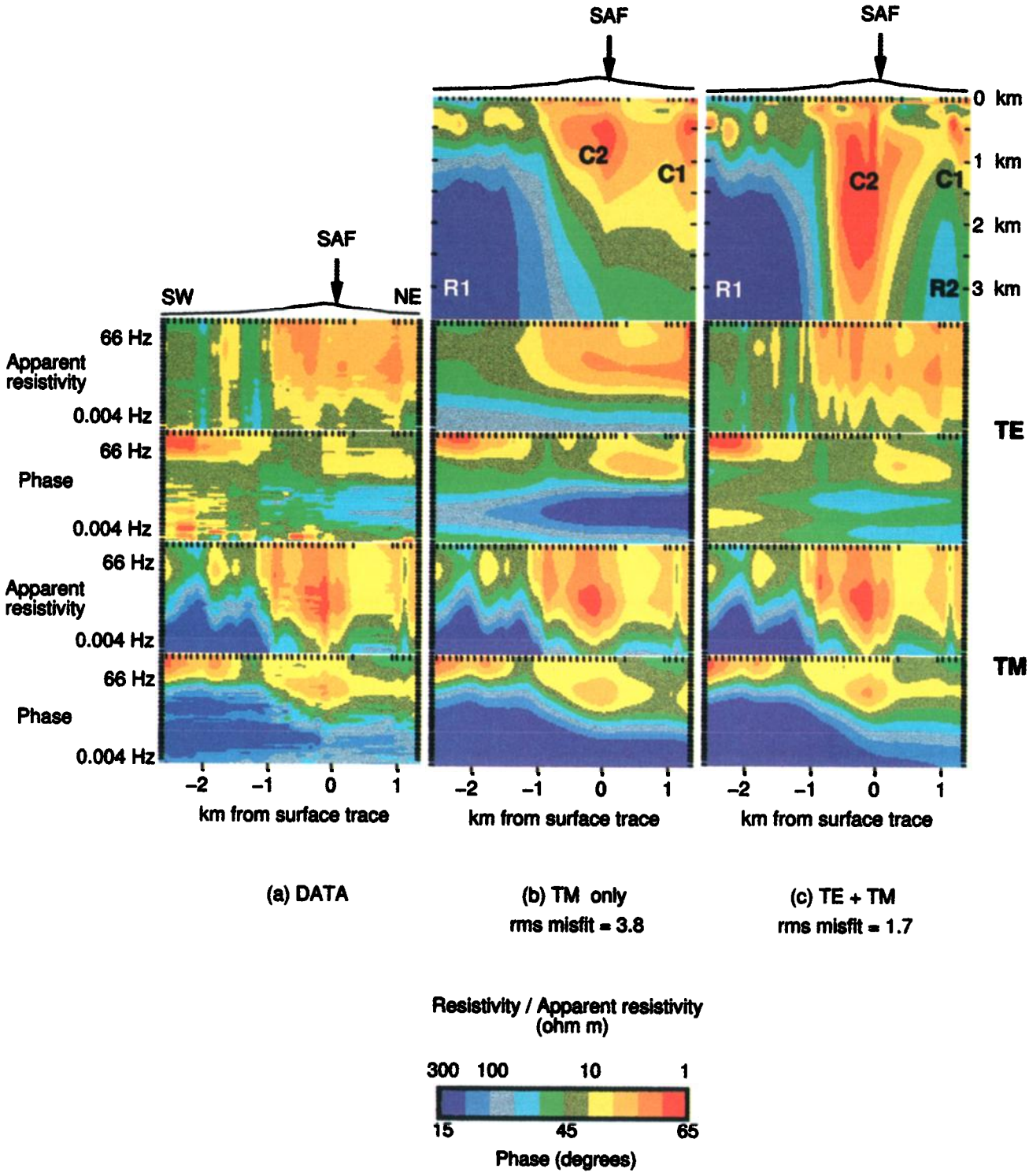

Plate 3. (a) Data pseudo-sections for the Parkfield MT profile and (b) model and response obtained by inverting the TM data. (c) Model and responses obtained by inverting and modeling both TE and TM mode data. Models and topography are plotted with no vertical exaggeration.

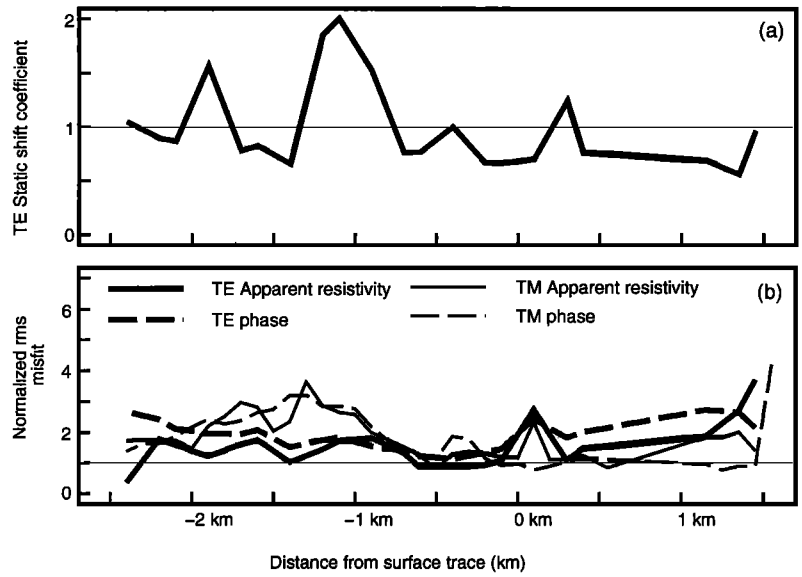

Figure 11. (a) Estimated TE mode static shift coefficients for Parkfield data. (b) Misfit between data and predicted response of model Plate 3c as a function of distance from the surface trace.

as this mode can be more susceptible to contamination by 3-D effects than the TM mode. Since the inclusion of the TE mode data significantly effects the inversion results for Parkfield, the possibility of 3-D effects needs careful consideration here. There are several lines of evidence that support a 2-D interpretation of this segment of the SAF. First, the higher-frequency data which we emphasize in the inversion fit a distorted 2-D model quite well, with a nearly fault-parallel geoelectric strike. Impedance skews are small (< 0.2) at all frequencies. Thus there is no evidence in the data itself for 3-D effects. Furthermore, additional MT profile data were collected on Middle Mountain in late 1997. Profiles to the northwest and southeast of the 1994 line interpreted here show similar resistivity and phase data [*Unsworth et al.*, 1997b]. Vertical magnetic field data can provide a useful indication of the connectivity of conductors along strike. Vertical field data were not collected in the 1994 survey but were collected in the 1997 survey. The induction vectors from this survey are generally normal to the fault zone, again consistent with a 2-D geoelectric structure with fault-parallel strike. Furthermore, vertical field data from a fault-normal profile some 3 km northwest of the 1994 profile closely match the vertical fields predicted by the 2-D model of Plate 3c down to 0.2 Hz. All of these observation are consistent with a 2-D interpretation, and none provide direct evidence for 3-D complications. Thus, while we cannot completely dismiss the possibility that 3-D effects may bias quantitative estimates of fault zone conductance, we believe that a 2-D interpretation incorporating TE phase data is not unreasonable in this case.

Having given substantial evidence that the fault zone is relatively 2-D, we will now demonstrate that a conductor within the fault zone is required to fit the TE mode data. Further forward models were computed to see how sensitive the data were to the depth extent of the fault zone conductor. Figure 12 shows the responses at site 21 of models derived from the TE+TM model shown in Plate 3c. The response at this site is observed at sites 16 to 25 and is clearly not a single-site anomaly. In models 24 and 23 the conductor is terminated at shallower depths, resulting in a minimum in Φ_{TE} at around 1 Hz and a rapidly rising ρ_{TE} which are not observed in the data. This is particularly true when the conductive zone is truncated at only 1 km depth (model 24). Model 23, which extends the fault zone conductor to 2 km depth, gives a comparable fit to the model with a conductor extending to 3 km. Extending the fault zone to a depth of 10 km in the presence of the eastern conductor (model 25) produces Φ_{TE} that is too high and ρ_{TE} that are too low. Thus the TE data indicate that the strong conductor extends to a depth of 2-4 km but does not continue to significantly greater depth. Note that termination at 2 km is possible, but the best fit to this data occurs with ~3 km depth extent. As with the models considered in Figure 7, the TM responses of these models are essentially indistinguishable.

The requirement for the moderately resistive zone (R2) east of the SAF was examined by replacing the resistor with a 10 Ω m zone. This altered Φ_{TM} by $\sim 5°$ east of of the SAF and indicates our data are sensitive to this zone. If observed at just one MT site, this anomaly might be disregarded as a single-site anomaly. However, in the continuous MT profiling data presented in this paper, we see such features in multiple sites. This redundancy in spatial sampling allows small features in the data to be interpreted with more confidence that that obtained with widely spaced sites.

Our preferred model consists of a conducting wedge (C2) that pinches out at around 2-4 km, with a weak conductive root present below that depth. However,

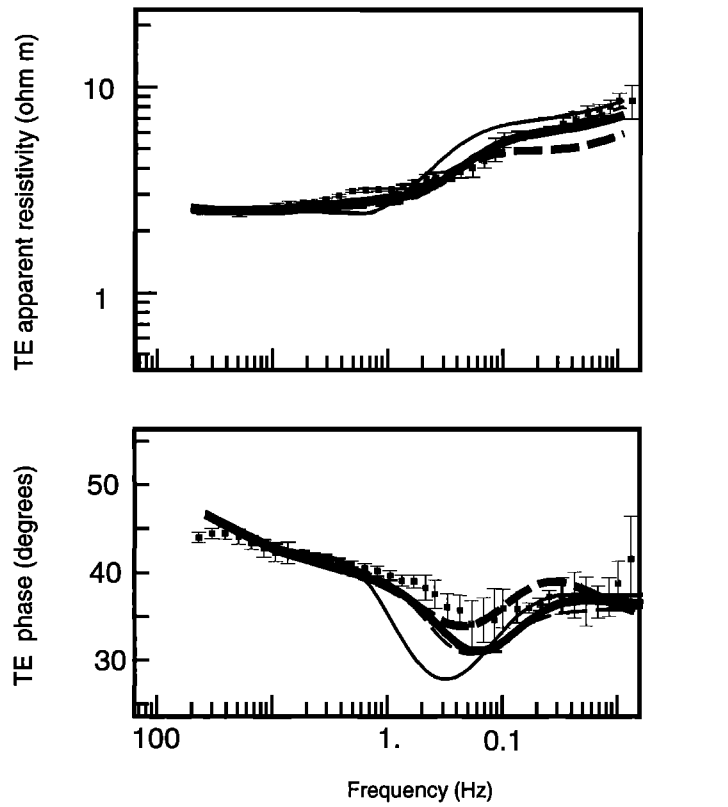

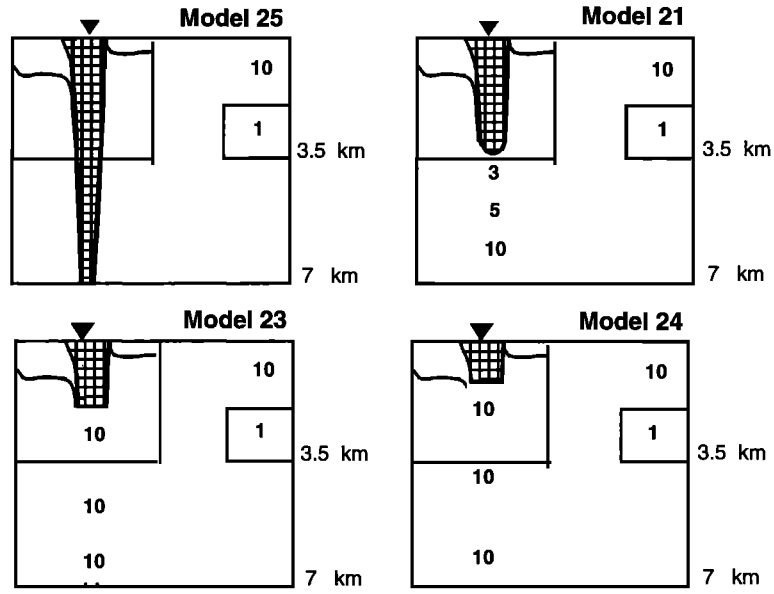

Figure 12. TE responses at dipole 21 for a set of models with the fault zone conductor terminating at depths of 1 km, 2 km, 3 km, and 10 km. These results demonstrate that if the geoelectric structure is 2-D, then the low-resistivity zone beneath the surface fault trace extends to a depth of 2-4 km. Resistivity models are shown with no vertical exaggeration.

the presence of the deeper root below 4 km is not constrained by the MT data, as shown by resolution analysis using synthetic MT data [*Eberhart-Phillips et al.*, 1995]. Low resistivities below 4-5 km in our model at depth in the fault zone could be an artifact caused by vertical smoothing of the regularized inversion.

4.3. Interpretation of the Middle Mountain Model

A detailed interpretation of the near-surface portion of the model has been given previously by *Unsworth et al.* [1997a]. This showed that the fault zone was characterized by a positive flower structure with a strong central conductor, interpreted as a fluid saturated zone of breccia at the core of fault. In this paper we have reexamined the prominent fault zone conductor more carefully and shown that the TE data are consistent with a conductive fault zone that pinches out over the depth range 2-4 km (assuming that the fault zone is sufficiently 2-D to allow interpretation of the TE mode). Given the nonuniqueness inherent in the inversion of magnetotelluric data, variants on this model may also reproduce the data. Clearly, alternate conductivity distributions may be possible east of the profile, given the lack of data in this area. The following major features are required by the TM mode data: (R1) a resistive block west of SAF and (C1) a conductive zone east extending east of the profile. These features can be considered a minimum structure model that is required by the TM data. However, as we have shown, 3-D effects appear to be small. Thus the combined TE and TM mode data can be used to add a resistive zone east of the fault (R2) and a vertical conductor in the fault zone (C2).

A revised interpretation, based on comparison to the geological map of *Sims* [1990], is shown in Plate 2b on the same scale as the Carrizo Plain interpretation. The unit R1 is interpreted as being granite of the Salinian block. The fault that bounds the east side of C2 is clearly the Gold Hill Thrust Fault. Resistor R2 is coincident with the anticline between the Parkfield syncline and the Gold Hill Thrust Fault. Is the relatively high resistivity of this feature reasonable given the high salinity of fluids that are widespread in the Franciscan formation [*Eberhart-Phillips and Michael*, 1993]? *Unsworth et al.* [1997a] used Archie's law to estimate the porosity required to account for the low resistivity in the core of the fault zone. At a depth of 3 km, a porosity in the range of ~10-30% was required within the fault zone to account for the low resistivity on the basis of fluids alone. Assuming the same pore fluid salinity, porosities in R2 would be in the range 1-10%, where upper and lower limits correspond to exponents of 2 and 1, respectively, in Archie's law. *Sims* [1990] shows that the area denoted as (R2) in our interpretation has Franciscan formation at its core at a depth of ~ 2 km. Given the heterogeneity of the Franciscan formation the inferred porosity is not unreasonable.

The two models shown in Plate 3 could be considered end-members of a spectrum of models consistent with the TM data. Depending on how much weight is given to the TE data, the fault zone conductor will have varying conductance. If the TE data are considered unreliable, then it will be restricted to the upper kilometer. However, if the TE data are deemed reliable and can be interpreted in a 2-D context, a fault zone conductor extending to a depth of 2-4 km is required by the data. Note once again that a conductor terminating as shallow as 2 km on Middle Mountain is a possibility. Both models in Plate 3 have related hydrogeological interpretations. In the first, fluid flows to the surface along the interface between the Franciscan, while in the second, fluids accumulate in a wide damaged zone of high porosity produced by fracturing of country rock.

The earthquake hypocenters in Plate 2b appear to lie on the west side of the fault zone conductor. However, when these events were relocated [*Ellsworth*, 1996], they were found to lie some 200 m east and 400 m deeper than the locations (from the Berkeley Seismic Station) shown in Plate 2b. Thus it is unclear whether the microearthquakes are in the center or on the edge of C2. In either case they are located within a conductive, presumably high fluid content fault zone, which stands in contrast to the seismically inactive and comparatively more resistive fault zone at Carrizo Plain.

The depth extent of the fluid saturated zone implied by the model of Plate 2b agrees well with the model of *Anderson et al.* [1987] based on the mapping of exhumed faults. In both, the zone of breccia terminates around 5 km depth. The MT image is also consistent with recent seismic tomography data which shows a 500 m wide seismic low-velocity zone extending to a depth of around 4 km beneath Middle Mountain (C. Thurber, personal communication, 1997). The presence of fluid lowers both electrical resistivity and the seismic velocity and is a natural explanation for the structures imaged by both datasets.

5. Discussion and Conclusions

On both MT profiles we have imaged narrow fault zone conductors extending to depths of 2-4 km and sharp variations of resistivity across the fault contact. The high-density electric field sampling has also allowed us to resolve many details of near-surface resistivity structure, along with variations in depth to the resistive basement. Although there are broad similarities in the two resistivity models of Plates 2a and 2b, there are also some very significant differences. These include (1) the contrast of resistivity across the fault; at Carrizo this is small with 1000+ Ω m material on each side, and at Parkfield there is a west to east change from 1000 to 30 Ω m; (2) the magnitude of the low resistivity anomaly in the fault zone; at 3 km depth fault zone conductance at Carrizo Plain is ~20 S, while at Parkfield our analy-

sis suggests a conductance of approximately 200 S; and (3) the width of the damaged zone at the core of the fault (as inferred from resistivity contrasts) is less than 300 m at Carrizo Plain and around 600 m at Parkfield.

These segments also have very different patterns of seismicity. Even though we are not imaging fault structure to the depth of the $M \approx 6$ events at Parkfield or the larger events that may periodically rupture the Carrizo segment, our resistivity data are sampling depths where shallow seismicity is present at Parkfield but absent at Carrizo Plain. How might the differences observed in the resistivity sections be related to the differences in seismicity?

First, could difference (1), the contrast in structure across the fault, contribute to the observed pattern of seismicity? Our results show that at Carrizo Plain, resistive, presumably crystalline, rocks are present on both sides of the fault. This is supported by the results of *Castillo and Hickman* [1995], who used stress analysis to show that the Carrizo segment is locally strong, in contrast to the general weakness of the fault documented by *Zoback et al.* [1987]. While the top of the resistive zone is deeper on the west side of the fault than on the east, these mechanically strong blocks may give the fault zone increased strength, compared to other parts of the San Andreas Fault. At Parkfield the situation is quite different with a resistive block of Salinian granite west of the fault and an electrically conductive, presumably fluid rich, and possibly mechanically weaker Franciscan complex to the east. Weak materials east of the fault could limit the strength of the fault and result in a cycle of more frequent, smaller earthquakes than is observed at Carrizo Plain.

Alternatively, it could be difference 2, the properties of the fault zone, specifically the fluid distribution, that are controlling seismicity. At Middle Mountain, Parkfield, a number of lines of evidence suggest that both shallow clusters of microearthquakes, and the characteristic deeper $M \approx 6$ events are fluid driven. *Johnson and McEvilly* [1995] suggested that earthquake clusters at Parkfield had focal mechanisms consistent with fluid cycling. At the depth of the characteristic $M \approx 6$ events a zone of low V_p and high V_p/V_s consistent with the presence of excess fluid has been reported [*Michelini and McEvilly,* 1991]. In contrast to Middle Mountain, Carrizo Plain is characterized by an almost complete absence of seismicity. In this paper we have shown that the conductance of the shallow (0-4 km) fault zone at Middle Mountain could be at least an order of magnitude greater than on the quiescent Carrizo Plain segment. This difference may be partly explained by fluid chemistry (i.e., the high salinity of 30,000 ppm chloride at Middle Mountain would produce a lower electrical resistivity than a lower salinity at Carrizo Plain). However, even with a high salinity of 30,000 ppm at Parkfield a porosity of $\sim$ 10% was required to explain the low resistivity. Thus we believe our data suggest higher porosities in the San Andreas Fault at Parkfield than at Carrizo Plain.

The possibility that seismicity is controlled by fluids in the fault has been proposed by many people. The correlation of fluid flow through the fault with abundant seismicity and creep was initially suggested by *Irwin and Barnes* [1975]. They proposed that these fluids originated in metamorphic reactions within the Franciscan formation and that fault creep occurs where Franciscan rocks abutted the fault and provided a ready supply of fluids. While we have considered only two locations on the San Andreas Fault system, our findings are consistent with this hypothesis.

The MT data for Parkfield and Carrizo Plain do not directly constrain structure at depths where the large earthquakes that periodically rupture this segment nucleate. If the hypothesis of *Irwin and Barnes* [1975] is correct and fluids enter at depths below 10 km and then flow to the surface, the high concentration of fluids in the near-surface at Parkfield may be indicative of an ample fluid supply at depth. Alternatively, the fluids may be entering the fault at shallow depths and be unrelated to the characteristic earthquakes. The resistor east of the SAF (R2) does not necessarily represent a barrier to fluid flow, rather just a zone of lower porosity with the Franciscan formation. At Carrizo Plain the absence of fluids in the near-surface may indicate a relatively dry fault zone at depth.

In reality, a combination of factors is probably responsible for the differences in seismic behavior of the two fault segments. We have shown that there are major differences in geoelectric structure between the Parkfield and Carrizo segments. Our results are consistent with previous surveys of both fault segments, but close to the fault, higher resolution of shallow structure is facilitated by dense spatial sampling. Subject to the absence of 3-D effects, our interpretation of the data is that the San Andreas Fault at Parkfield has a high-porosity core, while at Carrizo Plain the fault is essentially dry. Significantly, microearthquakes occur in the shallow fault zone at Parkfield but not at Carrizo Plain. Given careful analysis, we believe that MT exploration can provide valuable new constraints on the physical conditions within active fault zones.

Acknowledgments. Fieldwork was made possible by Wang Fei, Yang Yangjing, Weerachai Siripunvaraporn, Nong Wu, Xinghua Pu, Zhiyi Zhang, Yuval Zudman, and Arnell Dionosio. The staff of the BLM in Bakersfield, notably Johna Cochran, Judi Weaser and Larry Vredenburgh, are thanked for administrative and logistic support. The Nature Conservancy is thanked for letting us stay at the Painted Rock Ranch on Carrizo Plain, and Tony and George were most helpful hosts. Many private landowners at Carrizo Plain are thanked for access to their land, as are Kevin Kester and Jack Varian at Parkfield. Tom Burdette is thanked for help with permitting. This work was supported by NSF grant EAR-93-16160 and U.S. Geological Survey National Earthquake hazard reduction program grant 1434-94-6-2423. The development of the magnetotelluric inversion code was supported by U.S. Department of Energy grant DE-FG06-92-ER14231. Development of data processing code was supported by U.S. Department of Energy grant DE-FG06-92-ER14277. The authors acknowl-

edge many helpful discussions with Randy Mackie, Peter Malin, and members of the Parkfield working group. The manuscript benefited from reviews by Steve Park, Dal Stanley, and George Jiracek.

References

Anderson, J.L., R.H. Osborne, and D.E. Palmer, Cataclastic rocks of the San Gabriel fault- an expression of deformation at deeper crustal levels in the San Andreas Fault, *Tectonophysics, 98*, 209-251, 1987.

Arrowsmith, J.R., Coupled tectonic deformation and geomorphic degradation along the San Andreas Fault system, PhD. dissertation, 347 pp., Stanford Univ., Stanford, Calif., 1995.

Bakun W. H., and A. G. Lindh, The Parkfield, California, earthquake prediction experiment, *Science, 229*, 619-624, 1985.

Biasi, G.P., S.K. Park, R.L. Mackie, and T.R. Madden, Magnetotelluric studies in central California, paper presented at IAGA 10th Induction Workshop, Int. Assoc. of Geomagn. and Aeron., Ensenada, Mexico, 1990.

Brune, J.N., T.L. Henyey, and R.F. Roy, Heat flow, stress, and rate of slip along the San Andreas Fault, California, *J. Geophys. Res., 74*, 3821-3827, 1969.

Byerlee, J., Friction of rocks, *Pure Appl. Geophys., 116*, 615-625, 1978.

Byerlee, J., Friction, overpressure and fault normal compression, *Geophys. Res. Lett., 17*, 2109-2122, 1990.

Byerlee, J., Model for episodic flow of high-pressure water in fault zones before earthquakes, *Geology, 21*, 303-306, 1993.

Castillo, D.A., and S. Hickman, Near field stress and pore pressure observations along the Carrizo Plain segment of the San Andreas Fault, *Eos Trans. AGU, 76*(46), Fall Meet. Suppl., F360, 1995.

Chave, A.D., and J.T. Smith, On electric and magnetic galvanic distortion tensor decompositions, *J. Geophys. Res., 99*, 4669-4682, 1994.

Chester, F.M., J.P. Evans, and R.L. Biegel, Internal structure and weakening mechanisms of the San Andreas Fault, *J. Geophys. Res., 98*, 771-786, 1993.

Colburn, R.H., and W.D. Mooney, Two-dimensional velocity structure along the synclinal axis of the Great Valley, California, *Bull. Seismol. Soc. Am., 76*, 1305-1322, 1986.

Davis, T.L., M.B. Lagoe, W.J.M. Bazeley, S. Gordon, K. McIntosh and J.S. Namson, Structure of the Cuyama Valley, Caliente Range and Carrizo Plain and its significance to the structural style of the Southern Coast Ranges and Western Transverse Ranges, in *Tertiary Tectonics and Sedimentation of the Cuyama Basin, San Luis Obispo, Santa Barbara and Ventura Counties, California*, edited by W.J.M. Bazeley, pp. 141-158, Pac. Sec. Soc. of Econ. and Paleontol. Mineral., Bakersfield, Calif., 1988.

Dibblee, T W., Regional geologic map of San Andreas and related faults in Carrizo Plain, Temblor, Caliente and La Panza ranges and vicinity, California, *U.S. Geol. Surv. Misc. Field Invest. Map, I-757*, 1973a.

Dibblee, T.W., Stratigraphy of the Southern Coast ranges near the San Andreas Fault from Cholame to Maricopa, California, *U.S. Geol. Surv. Prof. Pap., 764*, 1973b.

Eberhart-Phillips, D., and A.J. Michael, Three-dimensional velocity structure, seismicity, and fault structure in the Parkfield Region, Central California, *J. Geophys. Res., 98*, 15,737-15,578, 1993.

Eberhart-Phillips, D., W.D. Stanley, B.D. Rodriguez, and W.J. Lutter, Surface seismic and electrical methods to detect fluids related to faulting, *J. Geophys. Res., 100*, 12,919-12,936, 1995.

Egbert, G.D., Robust multiple station magnetotelluric data processing, *Geophys. J. Int.,130*, 475-496, 1997.

Egbert, G.D., and J.R. Booker, Robust estimation of geomagnetic transfer functions, *Geophys. J. R. Astron. Soc., 87*, 173-194, 1986.

Ellsworth, W.L., Drilling into the Earthquake source: The search for a site to test theories of Earthquake Generation at Parkfield, paper presented at 8^{th} International Symposium on the Observation of the Continental Crust Through Drilling, Geol. Surv. of Jpn., Tsukuba, 1996.

Fishburn, M.D., Results of Deep Drilling, Elk Hills Field, Kern County, California, in *Structure, Stratigraphy and Hydrocarbon Occurrences of the San Joaquin Basin, California*, edited by G.K. Kuespert and S.A. Reid, pp. 157-167, Pac. Sect., Am. Assoc. of Pet. Geol., Bakersfield, Calif., 1990.

Gamble, T.D., W.M. Goubau, and J. Clarke, Magnetotellurics with a remote reference, *Geophysics, 44*, 53-68, 1979.

Graff, L.B., Exploration drilling in the Carrizo Plain, in *Guidebook to the Geology of Carrizo Plain and San Andreas Fault*, p. 21-24, San Joaquin Geol. Soc., Bakersfield, Calif., 1962.

Hickman, S., M.D. Zoback, L. Younker, and W. Ellsworth, Deep scientific drilling in the San Andreas Fault zone, *Eos Trans. AGU, 75*, 137, 140-142, 1994.

Hill, D.P., J.P. Eaton, and L.M. Jones, Seismicity 1980-86, in *The San Andreas Fault system, California*, edited by R.E. Wallace, *U.S. Geol. Surv. Prof. Pap.*, 1515, 115-151, 1990.

Hubbert, M.K., and W.W. Rubey, Role of fluid pressure in mechanics of overthrust faulting, *Geol. Soc. Am. Bull., 70*, 115-166, 1959.

Irwin, I.P., Geology and plate tectonic development, in *The San Andreas Fault System, California*, edited by R.E. Wallace, *U.S. Geol. Surv. Prof. Pap., 1515*, 61-80, 1990.

Irwin, P.I., and I. Barnes, Effect of geologic structure and metamorphic fluids on seismic behavior of the San Andreas fault system in central and northern California, *Geology, 3*, 713-716, 1975.

Johnson, P. A., and T. V. McEvilly, Parkfield seismicity: Fluid driven?, *J. Geophys. Res., 100*, 12,937-12,950, 1995.

Lachenbruch, A.H., Frictional heating, fluid pressure and the resistance to fault motion, *J. Geophys. Res., 85*, 6097-6112, 1980.

Mackie, R.L., B.R. Bennett, and T.R. Madden, Long period magnetotelluric measurements near the central California coast: A land-locked view of the conductivity structure under the Pacific Ocean, *Geophys. J. R. Astron. Soc., 95*, 181-194, 1988.

Mackie, R.L., D.W. Livelybrooks, T.R. Madden, and J.C. Larsen, A magnetotelluric investigation of the San Andreas fault at Carrizo Plain California, *Geophys. Res. Lett., 24*, 1847-1850, 1997.

Michelini, A., and T.V. McEvilly, Seismological studies at Parkfield. I. Simultaneous inversion for velocity structure and hypocenters using B-splines parameterization, *Bull. Seismol. Soc. Am., 81*, 524-552, 1991.

Nadeau, B., W. Foxall, and T.V. McEvilly, Clustering and periodic recurrence of microearthquakes on the San Andreas Fault at Parkfield, California, *Science, 267*, 503-507, 1995.

Page, B.M., The southern Coast Ranges, in *The Geotectonic Development of California*, edited by W.G. Ernst, pp. 329-416, Prentice-Hall, Engelwood Cliffs, N.J., 1981.

Park, J., and A.D. Chave, On the estimation of magnetotelluric response functions using the singular value decomposition, *Geophys. J. R. Astron. Soc., 77*, 683-709, 1984.

Park, S. K. and D.V. Fitterman, Sensitivity of the telluric Monitoring array in Parkfield, California, to changes in resistivity, *J. Geophys. Res., 95*, 15,557-15,571, 1990.

Park, S.K., G.P. Biasi, R.L. Mackie and T.R. Madden, Mag-

netotelluric evidence for crustal suture zones bounding the southern Great Valley, California, *J. Geophys. Res., 96*, 353-376, 1991.

Ranganayaki, R. P., and T. R. Madden, Generalized thin sheet analysis in magnetotellurics: An extension of Price's analysis, *Geophys. J. R. Astron. Soc., 60*, 445-457, 1980.

Rice, J. R., Fault stress states, pore pressure distributions, and the weakness of the San Andreas fault, in *Earthquake Mechanisms and Transport Properties of Rocks, edited by B. Evans, and T. Wong*, pp. 475-503, Academic, San Diego, Calif., 1992.

Ross, D.C., Possible correlations of basement rocks across the San Andreas, San Gregorio-Hosgri and Rinconada-Reliz-King City faults, California, *U.S. Geol. Surv. Prof. Pap., 1317*, 1984.

Ryder, R.T., and A. Thomson, Tectonically controlled fan delta and submarine fan sedimentation of late Miocene age, southern Temblor Range, California, *U.S. Geol. Surv. Prof. Pap. 1442*, 1989.

Sibson, R.H., R. Francois, and K.H. Poulsen, High-angle reverse faults, fluid pressure cycling and mesothermal gold-quartz deposits, *Geology, 16*, 551-555, 1988.

Sims, J.D., Geologic map of the San Andreas Fault in the Parkfield 7.5-minute quadrangle, Monterey and Fresno Counties, California, *U.S. Geol. Surv. Misc. Field Study Map, MF-2115*, 1990.

Sleep, N.H. and M.L. Blanpied, Creep, compaction and the weak rheology of major faults, *Nature, 359*, 687-692, 1992.

Smith, J. T., and J. R. Booker, Rapid inversion of two- and three-dimensional magnetotelluric data, *J. Geophys. Res., 96*, 3905-3922, 1991.

Torres-Verdin, C., and F.X. Bostick Jr., Principles of spatial surface electric field filtering in magnetotellurics: Electromagnetic array profiling (EMAP), *Geophysics, 57*, 603-622, 1992.

Unsworth, M. J., P. E. Malin, G. D. Egbert and J. R. Booker, Internal structure of the San Andreas Fault at Parkfield, California, *Geology, 25*, 359-362, 1997a.

Unsworth, M.J., P. Bedrosian, G.D. Egbert and M. Eisel, 3-D electrical resistivity structure of the San Andreas Fault at Parkfield, California, *Eos Trans. AGU, 78* (46), Fall Meet. Suppl., F696, 1997b.

Vedder, J.G., Geologic map of the Wells Ranch and Elkhorn Hills quadrangles, San Luis Obispo and Kern Counties, California, showing juxtaposed Cenozoic rock along the San Andreas fault, *U.S. Geol. Surv. Misc. Field Invest. Map, I-585*, 1970.

Wannamaker, P.E., G.W. Hohmann and S. Ward, Magnetotelluric responses of the three-dimensional bodies in layered earths, *Geophysics, 49*, 1517-1533, 1984.

Willcock, W.S.D., G.M. Purdy, and S.C. Solomon, Microearthquake evidence for extension across the Kane Transform fault, *J. Geophys. Res., 95*, 15,439-15,462, 1990.

Zoback, M.D., et al., New evidence on the state of stress of the San Andreas Fault system, *Science, 238*, 1105-1111, 1987.

J.R. Booker and M.J. Unsworth, Geophysics Program, University of Washington, Seattle, WA 98195. (unsworth@geophys.washington.edu)

G.D. Egbert, College of Oceanic and Atmospheric Sciences, Oregon State University, Corvallis, OR 97331-5503. (egbert@oce.orst.edu).

(Received May 23, 1997; revised February 13, 1998; accepted May 14, 1998.)